This Accepted Manuscript has not been copyedited and formatted. The final version may differ from this version. A link to any extended data will be provided when the final version is posted online.

eNeuro

Research Article: Methods/New Tools | Novel Tools and Methods

A Dynamic Clamp on Every Rig

A dynamic clamp on every rig

Niraj S. Desai, Richard Gray and Daniel Johnston

Center for Learning and Memory and Department of Neuroscience, the University of Texas at Austin, Austin, Texas 78712, United States

DOI: 10.1523/ENEURO.0250-17.2017

Received: 16 July 2017

Revised: 4 September 2017

Accepted: 11 September 2017

Published: 18 September 2017

Author contributions: N.S.D., R.G., and D.J. designed research; N.S.D. and R.G. performed research; N.S.D. and R.G. analyzed data; N.S.D., R.G., and D.J. wrote the paper.

Funding: HHS | NIH | National Institute of Mental Health (NIMH)
100000025
MH094839

Funding: HHS | NIH | National Institute of Neurological Disorders and Stroke (NINDS)
100000065
NS084473

Funding: McKnight Foundation
100005270

Conflict of Interest: Authors report no conflict of interest.

NIH MH094839 and NS084473; McKnight Foundation.

Correspondence: Niraj S. Desai, Center for Learning and Memory, The University of Texas at Austin, Austin, Texas 78712, United States. Phone: 1-512-475-7928. E-mail: desai@utexas.edu

Cite as: eNeuro 2017; 10.1523/ENEURO.0250-17.2017

Alerts: Sign up at eneuro.org/alerts to receive customized email alerts when the fully formatted version of this article is published.

Accepted manuscripts are peer-reviewed but have not been through the copyediting, formatting, or proofreading process.

Copyright © 2017 Desai et al.
This is an open-access article distributed under the terms of the Creative Commons Attribution 4.0 International license, which permits unrestricted use, distribution and reproduction in any medium provided that the original work is properly attributed.

eNeuro Accepted Manuscript

eNeuro Accepted Manuscript

1. Manuscript title

A dynamic clamp on every rig

2. Abbreviated title

A dynamic clamp on every rig

3. Author names and affiliations

Niraj S. Desai, Richard Gray, and Daniel Johnston

Center for Learning and Memory and Department of Neuroscience, The University of Texas at Austin, Austin, Texas 78712, United States

4. Author contributions

Designed research: NSD, RG, DJ
Performed research: NSD, RG
Analyzed data: NSD, RG
Wrote the paper: NSD, RG, DJ

5. Correspondence

Niraj S. Desai, Center for Learning and Memory, The University of Texas at Austin, Austin, Texas 78712, United States. Phone: 1-512-475-7928. E-mail: desai@utexas.edu.

6. Number of figures: 9

7. Number of tables: 0

8. Number of multimedia: 0

9. Number of words in abstract: 203

10. Number of words in significance statement: 86

11. Number of words in introduction: 623

12. Number of words in discussion: 1119

13. Acknowledgments

We are grateful to Elizabeth Arnold, Lauren Hewitt, and Gregory Ordemann for building dynamic clamp systems in order to test and improve the assembly instructions.

14. Conflict of interest: Authors report no conflict of interest.

15. Funding sources: NIH MH094839 and NS084473; McKnight Foundation.

eNeuro Accepted Manuscript

ABSTRACT

The dynamic clamp should be a standard part of every cellular electrophysiologist's toolbox. That it is not, even 25 years after its introduction, comes down to three issues: money, the disruption that adding dynamic clamp to an existing electrophysiology rig entails, and the technical prowess required of experimenters. These have been valid and limiting issues in the past, but no longer. Technological advances associated with the so-called "maker movement" render them moot. We demonstrate this by implementing a fast (~100 kHz) dynamic clamp system using an inexpensive microcontroller (Teensy 3.6). The overall cost of the system is less than USD$100, and assembling it requires no prior electronics experience. Modifying it – for example, to add Hodgkin-Huxley-style conductances – requires no prior programming experience. The system works together with existing electrophysiology data acquisition systems (for Macintosh, Windows, and Linux); it does not attempt to supplant them. Moreover, the process of assembling, modifying, and using the system constitutes a useful pedagogical exercise for students and researchers with no background but an interest in electronics and programming. We demonstrate the system's utility by implementing conductances as fast as a transient sodium conductance and as complex as the Ornstein-Uhlenbeck conductances of the "point conductance" model of synaptic background activity.

eNeuro Accepted Manuscript

47 **SIGNIFICANCE STATEMENT**

48

49 We describe a system for adding dynamic clamp capability to any existing intracellular electrophysiology
50 rig. Built around a simple microcontroller, the addition is inexpensive (<USD$100), can be used in
51 parallel with existing data acquisition systems (and hence entails no disruption of existing experiments),
52 and does not require any technical experience that a typical neuroscientist is unlikely to possess. Its
53 performance is comparable in speed and accuracy to the leading alternatives. This system should make
54 the dynamic clamp method accessible to a wide range of cellular electrophysiologists.

eNeuro Accepted Manuscript

INTRODUCTION

Current clamp and voltage clamp are the standard configurations of cellular electrophysiology. Every trained electrophysiologist is familiar with their properties, and every standard electrophysiological system incorporates them. And yet there is a third extant and potentially useful configuration: dynamic clamp (a.k.a., conductance clamp) (Prinz et al., 2004; Destexhe and Bal, 2009; Prinz and Cudmore, 2011). Introduced independently and concurrently by Sharp, Abbott, and Marder (Sharp et al., 1992, 1993) and Robinson and Kawai (1993), dynamic clamp is grounded in the idea that the effects that voltage-gated and ligand-gated channels have on a neuron's membrane potential can best be understood as changes in *conductance* rather than in *current*. The shift in emphasis requires that the electrophysiological system monitor membrane potential and use it, in real time, to calculate what current simulated channels would have passed had they been physically present.

The idea of dynamic clamp is simple, but how to implement it is not. The stumbling block is that dynamic clamp calculations must be done in *real time*, which is to say faster than any meaningful changes in channel properties or in membrane potential. In mammalian cortex, this means (much) faster than 10 kHz. A wide variety of implementations have been proposed since the earliest years, utilizing technically sophisticated manipulations of hardware and/or software (Biró and Giugliano, 2015; Clausen et al., 2013; Desai et al., 2006; Dorval et al., 2001; Kemenes et al., 2011; Kullmann et al, 2004; Milescu et al., 2008; Nowotny et al., 2006; Olypher et al., 2006; Ortega et al., 2014; Pinto et al., 2001; Raikov et al., 2004; Yang et al., 2015). These efforts have been useful and have had a broad impact, but they have not established dynamic clamp as a part of the standard repertoire of contemporary cellular electrophysiology. The limiting issues have been cost (as much as USD$6000 in one case), the requirement in other cases that existing data acquisition systems be replaced or substantially modified

eNeuro Accepted Manuscript

rather than merely supplemented, and the technical demands (e.g., use of a digital signal processing board or facility with C++ or real-time Linux) required of users in still other cases.

These limiting issues have all been valid heretofore, but (we would argue) they are no longer. The present decade has witnessed an explosion of projects designed to enable non-engineers and other non-specialists interested in building tools and other useful objects to make use of modern technological advances (Anderson 2014; Finley 2014; Morozov 2014). The Arduino microcontroller, in the field of embedded electronics, is perhaps the premier example (https://www.arduino.cc). Collectively called the "maker movement," these projects have already had a substantial impact in multiple areas of modern neuroscience, including multielectrode electrophysiology, imaging, behavioral neuroscience, and automated patch clamping (Baden et al., 2015; Desai et al., 2015; Potter et al., 2014; Siegle et al., 2017; Teikari et al., 2012).

In this paper, we demonstrate that one product of the maker movement – a microcontroller called the Teensy 3.6 (https://www.pjrc.com) – can be used to add dynamic clamp capability to any intracellular electrophysiology rig (whether for patch or sharp electrodes). The addition is cheap (less than USD$100), can be used in parallel with existing data acquisition systems (and hence entails no disruption of existing experiments), and does not require any technical experience that a typical neuroscience graduate student is unlikely to possess. Indeed, the process of building and using the system will likely teach novices and even moderately experienced researchers some useful things about electronics and programming, as well as initiating them into the potential of other maker movement projects. We demonstrate that the system can handle conductances as fast as a transient Hodgkin-Huxley-style sodium conductance and as complex as the Ornstein-Uhlenbeck conductances of the "point conductance" model of synaptic background activity (Destexhe et al., 2001).

eNeuro Accepted Manuscript

METHODS

A schematic overview of the system is given in Figure 1A.

The portions in black are present on every intracellular electrophysiology rig: an amplifier and a data acquisition (DAQ) board. The amplifier could be a Multiclamp 700B, a Dagan BVC-700A, a HEKA EPC-10, an AM Systems 2400, or any other amplifier that monitors a neuron's membrane potential and injects current into that neuron through a patch or sharp electrode. The DAQ board could be a Molecular Devices Digidata 1500, a HEKA ITC-18, a National Instruments PCIe-6343, or any of a huge number of other boards that work with Macintosh, Windows, or Linux operating systems; our dynamic clamp system places no constraint in this regard. We assume that the DAQ board is controlled on the host computer by a DAQ system suitable for intracellular electrophysiology. The system could be one of the commercial systems on the market (e.g., Molecular Devices pClamp 10 or AxoGraph) or it could be open source (e.g., Janelia's Wavesurfer) or it could be homemade. The point is simply that the electrophysiology rig already includes the components necessary to patch or impale neurons and record current clamp data.

Into this existing, working configuration, we insert the portion of Figure 1A depicted in red. It consists of a Teensy 3.6 microcontroller and associated electronics. We chose the microcontroller because, compared to other devices of its class and in its price range, it is fast (180 MHz clock speed), has substantial memory (256 kB RAM), and has a floating point unit (more on this in the Discussion). The Teensy is responsible in our system for performing all the dynamic clamp calculations. It determines, moment by moment, what current a voltage- or ligand-gated conductance would pass were it physically present and adds this to the current that the existing DAQ system has been instructed to inject (e.g., a

eNeuro Accepted Manuscript

family of current steps). That is, the existing DAQ system continues to perform all the standard current clamp (or voltage clamp) functions. The Teensy system simply adds a dynamic clamp component – it adds the current from simulated conductances to the current that the existing current clamp system specifies.

For the Teensy to do this, some electronic additions are required (Figure 1B): (1) a power supply, (2) circuitry to map the voltage output of the intracellular amplifier (typically ±9 V) representing the neuron's membrane potential to the voltages the Teensy can read (0-3.3 V), (3) electrical connections to and from the Teensy, (4) circuitry to transform the Teensy's output (0-3.3 V) into a voltage the intracellular amplifier can correctly interpret (typically ±9 V) as a current (in pA) to be injected into the neuron, and (5) circuitry to sum the dynamic clamp currents specified by the Teensy and the current clamp currents specified by the DAQ system. We explain these five additions, all of which can be built on a single solderless breadboard (Figure 1C), in the five sections that immediately follow.

After that, we discuss the software that controls the Teensy. While the Teensy 3.6 is not a microcontroller of the Arduino line (www.arduino.cc), it is very similar and can be programmed using the (open source) Arduino integrated development environment (IDE). We provide, in the online material, the code we used to program various simulated conductances; these serve as examples for users who might wish to program different simulated conductances. We also discuss code written in the (open source) Processing language (www.processing.org) to change dynamic clamp parameters "on the fly" (i.e., during a recording). Processing is a useful language because it is very simple and because, like Arduino, its code can be used without modification on all three major operating systems (Macintosh, Windows, Linux).

eNeuro Accepted Manuscript

We end the methods section by discussing how to calibrate the electronic components of the dynamic clamp system to ensure best performance.

Source code, a parts list, photographs, and step-by-step instructions are included in the Extended Data. Post-publication updates will be available at a website we have created for this purpose (dynamicclamp.com), with software archived at the public repository Github (https://github.com/nsdesai/dynamic_clamp)

Power supply

The power supply serves two purposes: it provides power for the operational amplifiers ("op-amps") of the other circuits and it provides the positive (negative) reference voltages the other circuits use to shift up (down) the voltages sent to (from) the Teensy microcontroller. For both these purposes, we require a positive voltage (approximately +9 V) and a negative voltage (approximately -9 V).

The simplest power source suitable for both purposes is an 18 V DC wall adaptor (colloquially called a "wall wart"). Such an adaptor typically terminates in a barrel plug that can be plugged into a barrel connector. (We provide a full parts list, including links to supplier webpages, in the Extended Data, so that readers can see for themselves what all the parts look like.) This power source cannot work alone because it is positive only, whereas we wish to have both positive and negative voltages. More precisely, we wish to break up the +18 V into one rail at +9 V, one rail at -9 V, with a ground (called a "virtual ground") right at the halfway point.

Circuits that perform this function are called "rail splitters." In principle, a purely passive rail splitter circuit – essentially a voltage divider – would suffice here, but in this design we opted for an op-amp

eNeuro Accepted Manuscript

circuit, because it minimizes asymmetry between the positive and negative rails and buffers the power supply from the downstream circuits. (Keeping one part of the system from interfering with other parts – "buffering" – is a general principle of electronic design.) The op-amp circuit we chose is a ubiquitous integrated circuit (IC) from Texas Instruments (TLE2426). Figure 2A shows schematically how the IC is connected.

In the Extended Data, we describe and show (with pictures) how the circuit looks when the parts are physically connected on a solderless breadboard. The breadboard has four power rails. One rail is marked +9 V and another is marked -9 V. The downstream circuits use these two rails to power their own op-amps and as reference points for +9 V and -9 V. A third rail on the breadboard is connected to the virtual ground of the rail splitter. Every other voltage in this system will be referenced to this ground rail.

Amplifier output to microcontroller input

An intracellular electrophysiology amplifier in current clamp mode monitors a neuron's membrane potential and outputs a signal representing this value. For real neurons, the membrane potential will be in a range no wider than -90 mV to +90 mV. The representative output will depend on the gain of the amplifier, but for the typical settings of commonly-used amplifiers the corresponding range will be -9 V to +9 V. This is too broad a range for the analog inputs of the Teensy microcontroller (or other controllers of this class), which are limited to 0 to 3.3 V.

To map ±9 V from the amplifier onto 0-3.3 V to the microcontroller, we employ three distinct elements (Fig. 2B). The first is a *follower* circuit. It takes an input (±9 V) and simply sends out an identical output (±9 V). The follower's purpose is to separate – buffer – the input from the output, to keep them from

eNeuro Accepted Manuscript

interfering with each other. The second is a *voltage divider* that transforms the voltage from the amplifier (±9 V) onto a more limited range (approximately ±1.6 mV, the precise numbers depend on the precise resistor values chosen). The third is a *differential amplifier* that adds (approximately) 1.6 V to shift the output of the second element into the range 0-3.2 V, which roughly matches the dynamic range of the Teensy's analog-to-digital (ADC) input.

One can calculate the relationship between the input (V_{IN}) to this three-element circuit and its output (V_{OUT}) by assuming that all the resistor values and power supply voltages are exact and that all the op-amps are ideal (Senturia and Wedlock, 1975). This is it:

$$V_{OUT} = (1 + \frac{R_6}{R_5})\left[\frac{R_4 R_2}{(R_3 + R_4)(R_1 + R_2)} V_{IN} + \frac{R_3}{(R_3 + R_4)} V_+\right]$$

In this equation , V_+ is the voltage of the positive power rail (+9 V). Note that the relationship between V_{IN} and V_{OUT} is *linear*. We constructed this circuit on a breadboard using resistor values between 100 Ω and 22 kΩ (specified in the figure caption) and an IC that contains two op-amps (LM358n). Testing the breadboard circuit, we found that the empirical relationship between V_{IN} and V_{OUT} was indeed strictly linear (see "Calibration" section below), but that the numerical values of the slope and intercept were somewhat different from what the exact equation would predict (by ~2%). This discrepancy resulted from imperfections in the (inexpensive) electronic components we chose and the non-ideal behavior of the op-amps of the LM358n chip.

Fortunately, the discrepancy can be corrected in software, without having to substitute better (and more expensive) electronic components. As explained in the "Calibration" section, this can be done by

eNeuro Accepted Manuscript

measuring V_{OUT} values in response to a range of known V_{IN} values. The numbers can be fitted to a straight line and the resulting slope and intercept used instead of the calculated slope and intercept.

Microcontroller connections

The output of the three-element circuit (now 0-3.2 V) is fed to an ADC input on the Teensy microcontroller (Fig. 2C). The Teensy 3.6 has 25 ADC inputs; our default software simply selects the first of these (A0, pin 14), but any can be used. The Teensy analog ground should be connected to the virtual ground defined by the rail splitter circuit. The Teensy has two digital-to-analog (DAC) outputs; our default software uses the first of these (A21).

Microcontroller output to amplifier input

The output of the Teensy DAC will be a voltage between 0 V and 3.3 V, but most amplifiers in current-clamp mode expect command voltages between -9 V and +9 V, with negative voltages representing hyperpolarizing current injections and positive voltages representing depolarizing current injections. Mapping 0-3.3 V onto the range ±9 V is the inverse of the problem we faced earlier, and its solution is similar but inverted. We use a differential amplifier both to shift 0-3.3 V down to the range ±1.65 V and to amplify the result (Fig. 2D).

Assuming perfect, ideal components, we can calculate the relationship between the input supplied by the Teensy (V_{DAC}) and the output of the circuit (V_{DC}, representing the dynamic clamp command signal) (Senturia and Wedlock, 1975):

$$V_{DC} = \left(1 + \frac{R_{10}}{R_9}\right)\left[\frac{R_8}{(R_7 + R_8)} V_{DAC} + \frac{R_7}{(R_7 + R_8)} V_{-}\right]$$

eNeuro Accepted Manuscript

Here, $V\_$ is the voltage of the negative power rail (-9 V). Again, the relationship between input (V_{DAC}) and output (V_{DC}) is linear. And again, when we constructed the circuit on a breadboard, we found that, while the empirical relationship between V_{DAC} and V_{DC} was linear, it was not strictly given by the calculated formula (off by ~2%). This discrepancy too can be resolved in software (see "Calibration" section).

Summing circuit

The fifth and last electronic circuit is designed to sum the dynamic clamp command voltage V_{DC} and the current clamp command voltage from the DAQ system V_{DAQ}. Summing voltages is a common electronics task, and we perform it in a standard fashion: an inverting amplifier that sums the two voltages but switches their polarity followed by a second inverting amplifier that switches the polarity back (Fig. 2E).

Software

Arduino IDE

There are multiple ways of programming the Teensy 3.6, including simply using the C language, but the most sensible way to do so is through the Arduino IDE (https://www.arduino.cc/en/Main/Software). Arduino has emerged over the last five years as the microcontroller of choice of the maker movement, including nearly all the neuroscience-related projects (Baden et al., 2015; Desai et al., 2015; Potter et al., 2014; Siegle et al., 2017). The Arduino IDE and its associated language retain the essential syntax of C while making the process of interfacing with a microcontroller straightforward. Although Teensy is not part of the Arduino line of microcontrollers, a Teensy-specific add-on to the Arduino IDE exists and

eNeuro Accepted Manuscript

allows one to use the IDE and most of its libraries (https://www.pjrc.com/teensy/teensyduino.html). Detailed installation and use instructions are included in the Extended Data.

We wrote our dynamic clamp software using the Arduino IDE. The code is contained in the Extended Data folder *dynamic_clamp* and the main file is called *dynamic_clamp.ino*. Opening the latter not only opens the main file but its associated files, which appear in separate tabs. Each tabbed file contains the code for a specific conductance. The main file is structured in three parts: global variables, a set-up function, and a loop function. The global variables are self-explanatory (variables needed by all and therefore accessible to all functions); the set-up function is run once when the program is uploaded to the board and does things like initialize serial communication between the host computer and the Teensy board; the loop function is run at every time step – it calls each of the conductance-specific tabbed files to get the current specified by that conductance.

In the example software, we coded five separate conductances: (1) a simple shunt conductance, (2) a hyperpolarization-activated cyclic nucleotide–gated (HCN) conductance (Gasparini et al., 2004), (3) a fast, transient sodium conductance (Johnston and Wu, 1994), (4) an excitatory postsynaptic conductance (EPSC) (Compte et al., 2000), and (5) “high conductance state” synaptic background conductances (Destexhe et al. 2001, 2003). The first is simple. The second and third are Hodgkin-Huxley conductances with one and four gates, respectively. The fourth is a synaptic conductance that is triggered by a TTL pulse sent by the DAQ board to the Teensy microcontroller. The fifth is comprised by two conductances – one excitatory, one inhibitory – generated by Ornstein-Uhlenbeck (OU) processes. Our example code demonstrates how to numerically integrate the stochastic OU equations and how to generate the Gaussian random numbers the OU processes require (Marsaglia and Bray, 1964). Together these five examples span the range of conductances users are likely to wish to employ, and this code is meant to provide templates from which users can create other conductances.

eNeuro Accepted Manuscript

As a further aid, in the Extended Data, we also describe step-by-step how to add a potassium M conductance (Fransen et al., 2002).

Processing

When the Arduino program is uploaded to the Teensy microcontroller, all of the dynamic clamp conductances are initialized to zero. They can be changed to non-zero values while the program is running. That is, the dynamic clamp conductances can be changed "on the fly" during a given recording.

The simplest way for the host computer to tell the microcontroller to modify the dynamic clamp conductances is through the USB port that connects them. In our default Arduino software, the microcontroller constantly checks for a serial communication from the host computer, and changes the conductance values as soon as it arrives. Unfortunately, the Arduino IDE itself has no good way of sending real-time communication from the host computer to the microcontroller. Fortunately, many other programs do. One called Processing (www.processing.org) is especially well suited for this purpose: it is an open-source environment with a simple syntax (based on Java and thus possessing a family resemblance to the C-like Arduino) that has a huge user base and is platform independent (Windows, Macintosh, Linux).

In the Extended Data, we include a Processing sketch (called *processing_control.pde*) that creates a graphical user interface (GUI) through which users can change the values of the maximal conductances (in nS) of the five conductances of our default software. The GUI also allows users to modify the diffusion constants (nS^2/ms) of the OU processes. All the parameters can be modified by moving the sliders in the GUI and pressing the "upload" button.

But there is nothing unique about Processing. Users are free to use any software they wish in order, for example, to couple their data acquisition and dynamic clamp software more tightly. To emphasize this

eNeuro Accepted Manuscript

point, we also include Matlab software (Windows, Macintosh, Linux) in the Extended Data that does the same things as the Processing sketch.

Calibration

Electronic components are typically specified with some margin of error (e.g., the specified resistance or capacitance will only be good to within 1%) and no op-amp or other active component behaves ideally. This means that the slope and intercept values for the electronic circuits calculated above will be not quite correct. Empirically, using the components specified in the parts list, we find that "not quite correct" means "not good enough."

Fortunately, the input-output functions of the circuits in question (Fig. 2B and 2D) are strictly linear (Fig. 3A). We determined this by directly measuring the output of the two circuits when they were subjected to a range of input voltages. In principle, users could do the same thing we did in that figure: use the DAQ board to send a voltage directly to the circuit input (Fig. 3A, left) or to measure the circuit output directly (Fig. 3A, right). But a slightly simpler method exists: attach a model cell to the headstage of the amplifier, measure the responses to a variety of current/voltage commands, and use these together with the model cell's known architecture (arrangement of resistances and capacitances) to calculate the calibration parameters. The model cell could be as simple as a single resistor, but in Figure 3B we used a Patch-1U model cell ("cell mode") attached to a Multiclamp 700B amplifier (Molecular Devices). In cell mode, this model cell incorporates two resistors, representing input resistance and series resistance, and two capacitors, representing membrane capacitance and stray capacitance (due to the glass electrode) (Fig. 3B).

In the Extended Data, we include a Processing sketch and step-by-step instructions for calibrating the system using a model cell attached to an amplifier.

eNeuro Accepted Manuscript

Testing

We mainly tested the dynamic clamp system using a Windows 10 computer, Multiclamp 700B amplifier (Molecular Devices), PCIe-6343 data acquisition board (National Instruments), Patch-1U model cell (Molecular Devices), and custom MATLAB (The Mathworks) data acquisition software. To check that the system was indeed independent of operating system and equipment type, we also tested it on a rig with a Mac OS X computer, an Axopatch 200B amplifier (Molecular Devices), an ITC-18 data acquisition board (HEKA Instruments), and custom Igor Pro (Wavemetrics) data acquisition software.

Where indicated, we replaced the model cell in our tests with whole cell patch clamp recordings from mouse layer 2/3 or 5 pyramidal neurons. The mice were C57BL/6 males (6-8 weeks old, Jackson Laboratory). Brain slices containing medial prefrontal cortex were prepared using standard procedures. Shortly after receiving a lethal dose of ketamine/xylazine, mice were perfused transcardially with an ice-cold solution containing (in mM): 2.5 KCl, 1.25 NaH_2PO_4, 25 $NaHCO_3$, 0.5 $CaCl_2$, 7 $MgCl_2$, 7 dextrose, 205 sucrose, 1.3 ascorbate, and 3 sodium pyruvate (bubbled with 95% O_2/5% CO_2 to maintain pH at ~7.4). Brains were removed, and a vibratome was used to make 300 µm thick coronal sections. Slices were cut in the same ice-cold saline used for perfusion and then were held for 30 min at 35°C in a chamber filled with artificial CSF containing (in mM): 125 NaCl, 2.5 KCl, 1.25 NaH_2PO_4, 25 $NaHCO_3$, 2 $CaCl_2$, 2 $MgCl_2$, 25 dextrose, 1.3 ascorbate, and 3 sodium pyruvate (bubbled with 95% O_2/5% CO_2). Thereafter, they were maintained at room temperature in the same solution. Patch clamp recordings were obtained under visual guidance at 35°C using patch electrodes (3-7 MΩ) filled with an internal solution containing (in mM): K-gluconate 125, KCl 10, NaCl 4, HEPES 10, Mg-ATP 4, Tris-GTP 0.3, and phosphocreatine 7 (pH 7.4 at physiological temperatures). All animal procedures were approved by the Institutional Animal Care

eNeuro Accepted Manuscript

and Use Committee of the University of Texas at Austin and were in accordance with National Institutes of Health guidelines.

Software accessibility

The software for the system is available, together with other useful materials (a parts list, assembly and use instructions, photographs), as Extended Data. These are also available at a website we have created for this purpose (dynamicclamp.com), with software archived by the public repository Github (https://github.com/nsdesai/dynamic_clamp). Any post-publication improvements to the hardware or software will be available at these sites.

eNeuro Accepted Manuscript

RESULTS

We validated the dynamic clamp system in two distinct but complementary ways: (1) with a model cell (Fig. 3B) attached to the amplifier headstage, and (2) with whole cell patch recordings from layer 2/3 or 5 pyramidal neurons in slices of mouse prefrontal cortex (6-8 weeks old). The first was our principal method because it provided a steady baseline against which the effects of added (simulated) conductance could be reliably contrasted. The second was useful because it more closely matched the experimental configuration in which potential users of this system are likely to be interested.

Timing

One question is important in both cases: how fast is the dynamic clamp? For a single simulated conductance, the answer approaches 100 kHz, with a jitter of <2 µs. We determined this by measuring the distribution of time steps for different dynamic clamp configurations (Fig. 3C, three left-most panels). Moreover, the time per cycle does not grow linearly with the number of simulated conductances, because most of the time cost (analog read + analog write) is fixed and common for all conductances. So, for example, simulating shunt, HCN, and sodium conductances at the same time can be done at better than 80 kHz (Figure 3C, second from left). In keeping with these numbers, the latency between membrane potential V_m and the dynamic clamp current was ~10 µs (Fig. 3C, right).

In principle, the system could be sped up by using less averaging when reading from an analog input or employing higher quality op-amps (with a larger bandwidth and slew rate). However, we found – and show in what follows – that the system as described and constructed can handle even the most challenging conductance (i.e., transient sodium) without difficulty. We discuss the potential speed improvements in the Discussion section.

eNeuro Accepted Manuscript

Model cell: shunt conductance

The simplest intrinsic conductance a neuron might possess is a shunt conductance, which is a constant conductance. The current it passes is the product of its amplitude and the driving force (the difference between the membrane potential and the conductance's reversal potential): $I = -g_{shunt}(V_m - E_{rev})$. In Figure 4, we added a shunt conductance to the model cell of Figure 3B; we used the amplifier's built-in bridge balance and capacitance compensation circuity to minimize the effects of series resistance and pipette capacitance. From the diagram, the equivalent circuit, after balance and compensation, should have been 500 MΩ in parallel with 33 pF. However, the components used to make up the model cell are far from ideal (see the Molecular Devices page on the model cell's precision: http://bit.ly/2qHavi1). By injecting a variety of time-varying currents, we found that the model cell's parameters were better fitted by resistance and capacitance values of 507.7 MΩ and 35.9 pF. We used these numbers to check the precision of our dynamic clamp currents.

In Figure 4, we injected a family of current steps (-50 to +50 pA) into the model cell. The model was simply a resistor in parallel with a capacitor (an "RC circuit"). We therefore expected and found that the voltage responses to the steps were exponential growth and decay. Adding +5 nS of shunt conductance preserved the basic shape of the responses – all the shunt conductance does is decrease the value of "R" – but it reduced the steady-state deflections and made the responses faster. To check the system's behavior quantitatively, we used a National Instruments DAQ board (50 kHz, 16 bit) to directly measure the dynamic clamp current emitted by the system and to compare it to the current that should have been passed given the recorded membrane potential had the system worked perfectly. These numbers (Fig. 4, upper right, measured vs. numerical) were in good agreement. The insert shows a histogram of the deviation (error) between the measured and numerical currents during the steps. The absolute

eNeuro Accepted Manuscript

value of the error averaged 0.2 ± 0.2 pA (mean ± SD). Moreover, when we varied the amplitude of the shunt conductance, the measured input resistances (lower left) and time constants (lower right, estimated by fitting single exponentials to the voltage responses to current steps) closely matched the correct values determined by numerical calculation. The average difference was less than 2%, and in no case was the difference more than 5%.

Model cell: HCN conductance

One step up in complexity from a shunt conductance is an intrinsic conductance with a single activation gate. Several such conductances are important physiologically, including delayed-rectifier potassium and the HCN conductance. Here we focus on the HCN conductance. It activates but does not inactivate. What makes the conductance unusual is that the proportion of activated channels is increased by *hyperpolarization* (Fig. 5A) and that the reversal potential sits near the base of the activation curve. This configuration imbues the HCN conductance with interesting physiological properties (Biel et al., 2009). The dynamics of the HCN conductance can be modeled by a single differential equation:

$$\frac{ds(t)}{dt} = -(s(t) - s_{inf}(V_m))/\tau_s(V_m)$$

where $s(t)$ represents the fraction of open HCN channels at any moment in time *t*, and $s_{inf}(V)$ and $\tau_s(V)$ are the voltage-dependent steady-state value and time constant, respectively (Fig. 5A) (Gasparini et al., 2004). Our dynamic clamp system integrated this equation using the forward Euler method with a time step of ~10 µs.

eNeuro Accepted Manuscript

How well it did this is shown in Figures 5B and 5C. Two important physiological signatures of an HCN conductance are *sag* and *resonance* (Biel et al., 2009). Adding a simulated HCN conductance to the model cell introduced a sag potential (Fig. 5B) when the model was subjected to hyperpolarizing current steps. (The baseline potential of the model cell here and below was set at a resting potential of -70 mV.) The HCN conductance also effectively added an inductance to the circuit (termed a "phenomenological inductance" by Narayanan and Johnston, 2008). This transformed the equivalent circuit of the model cell from an RC circuit to an RLC circuit: it transformed the cell from a lowpass filter into a bandpass filter, with a distinct resonance frequency (Fig. 5C).

More important than these qualitative effects was that the simulated currents were quantitatively correct. We directly measured the currents emitted by the dynamic clamp system and compared them to the currents specified by precise numerical integration (4th order Runge-Kutta, 10 µs time step) of the differential equation. The agreement was very good (Fig. 5B, 5C, and 5D); for both step currents and oscillating (chirp) currents, the average error (absolute value, mean ± SD) was less than 1 pA (steps: 0.7 ± 0.5 pA; oscillating: 0.4 ± 0.3 pA) and in no case was the absolute error ever greater than 2 pA.

Model cell: sodium conductance

The classical Hodgkin-Huxley formulation of the sodium conductance involves three identical and independent activation gates $m(t)$ and a single inactivation gate $h(t)$ (Johnston and Wu, 1994). The behavior of each is determined by a differential equation that involves voltage-dependent functions:

$$\frac{dm(t)}{dt} = -(m(t) - m_{inf}(V_m))/\tau_m(V_m)$$

eNeuro Accepted Manuscript

$$\frac{dh(t)}{dt} = -(h(t) - h_{inf}(V_m))/\tau_h(V_m)$$

448

449 The voltage-dependent functions are shown in Figure 6A. The sodium current is given by $I =$
450 $-g_{Na}m(t)^3h(t)(V_m - E_{rev})$, where g_{Na} is the maximal sodium conductance and E_{rev} = +50 mV is the
451 sodium reversal potential. Integrating these equations in real time is more challenging than in the HCN
452 case not only because there are now two equations rather than one, but because the characteristic time
453 associated with the activation gate $\tau_m(V)$ is very short (<0.5 ms). This sets the required time scale.

454 The microcontroller integrated these equations using the forward Euler method with a time step of <12
455 µs. To check that this was satisfactory, we simulated a voltage clamp experiment in which the model cell
456 was stepped instantly from -70 mV to 0 mV. The sodium current elicited by such a step can be written
457 down exactly. We compared the exact solution to those calculated using various numerical methods
458 (Fig. 6B). As expected, the 4th order Runge-Kutta method, which is widely used in modeling studies
459 because of its stability and precision (Bettencourt et al., 2008), matched the exact solution almost
460 perfectly. How well the forward Euler method did depended on the time step: time steps longer than
461 200 µs gave unstable solutions; those between 25 and 200 µs were stable but imprecise; but those less
462 than 25 µs were generally satisfactory. In particular, forward Euler with a time step of 12 µs and a jitter
463 of 2 µs, which matches the microcontroller's performance, differed from the exact solution only near
464 the peak of the sodium current and then only by a few percent (Fig. 6B, compare black and red traces).
465 This result suggests that, with the possible exception of some fine details of spike shape (Bettencourt et
466 al., 2008), forward Euler may be used to simulate Hodgkin-Huxley-style sodium conductances as long as
467 the time step is <25 µs – which is the case here.

468 We tested the dynamic clamp system's performance by using two types of stimuli (Figs. 6C and 6D): slow
469 current ramps (5-20 pA/s) and brief current steps (0-100 pA, 40 ms). In response to the ramps, the

eNeuro Accepted Manuscript

simulated sodium current activated and inactivated as expected (Fig. 6C, left); the match between the measured currents and those predicted by a precise numerical integration (4^{th} order Runge-Kutta, 10 µs time step) was very good – the absolute value of the error averaged 0.4 ± 0.3 pA (Fig. 6C, right). Even more striking was the response to brief current steps: these exhibited threshold behavior (Fig. 6D, left). Small currents (<25 pA) moved the model cell's potential only a small distance from its baseline of -70 mV, thus eliciting minimal sodium current. But larger currents (>50 pA) resulted in sharp, spike-like bursts of sodium current. In these latter cases, the deviation between the measured current and the current expected from a precise numerical integration could be as large as 9 pA (Fig. 6D, right, top). This error was still small relative to the size of the underlying currents (>300 pA), and it likely originated from small imperfections in the patch clamp amplifier settings. Sodium conductance is very sensitive to such deviations. For example, if the baseline potential had been off by 0.5 mV because the model cell's starting potential was not precisely -70 mV, that alone would have resulted in an error of the same shape and magnitude as the one we measured (Fig. 6D, right, bottom), without any contribution from the dynamic clamp system.

Model cell: EPSCs

Synaptic inputs to central neurons are mostly, although not exclusively, mediated by chemical synapses. These usually exhibit a rise time that is much faster than the decay time. There are several distinct ways of modeling the time course of synaptic currents, such as alpha functions and the difference of exponentials. Here we illustrate a particularly useful and general two-stage kinetic scheme (Destexhe et al., 1994; Compte et al., 2000; Walcott et al. 2011). We use it to model AMPA currents, but it is straightforward to modify it to model other types of synaptic currents. The kinetic scheme involves two variables:

eNeuro Accepted Manuscript

493

$$\frac{dx(t)}{dt} = -\frac{x(t)}{\tau_x} + \sum_i \delta(t - t_i)$$

$$\frac{ds(t)}{dt} = -\frac{s(t)}{\tau_s} + \alpha_s x(t)[1 - s(t)]$$

494

495 where α_s is a constant determining saturation properties; τ_s and τ_x are time constants controlling decay
496 and rise times, respectively; $\delta(t)$ is the Dirac delta function; and $\{t_i\}$ are the presynaptic spike times.
497 The resulting current is given by $I = -g_{syn}s(t)[V_m(t) - E_{rev}]$, where E_{rev} is the synaptic reversal
498 potential. To model AMPA currents, we set $E_{rev} = 0\ mV$, $\tau_s = 10\ ms$, $\tau_x = 1\ ms$, and $\alpha_s = 1\ ms^{-1}$.

499 The presynaptic spike times $\{t_i\}$ were determined by TTL triggers sent by the DAQ system. We sent
500 triggers at rates of 10, 20, and 50 Hz (Fig. 7A). The higher frequencies showed evidence of synaptic
501 summation. As was true of intrinsic conductances, the agreement between the measured dynamic
502 clamp currents and numerical estimates of ideal behavior was excellent (Fig. 7B). This agreement can be
503 quantified by considering a histogram of the errors, computed as the difference between the measured
504 and expected currents, with the latter derived from a precise numerical integration of the differential
505 equations (Fig. 7C). The average absolute error across all frequencies was 0.2 ± 0.2 pA (mean ± SD) ; the
506 largest errors, which occurred at the peaks of the EPSCs, were <1.5 pA.

507

508 ***Model cell: synaptic background activity***

509 Most electrophysiological studies of neuronal properties have been conducted *in vitro*, using
510 preparations like brain slices and cell cultures, where the electrical and chemical background can be
511 tightly controlled. However, neurons *in vivo* confront a rather different environment: they receive a

eNeuro Accepted Manuscript

continuous barrage of excitatory and inhibitory synaptic inputs, even in the absence of sensory or motor stimulation; a significant portion of total conductance is contributed by synaptic conductances rather than intrinsic ones; neurons are depolarized above rest by a much as 10 mV; and "resting" membrane potential fluctuates by as much as 5 mV (Steriade et al., 2001; Destexhe et al., 2003). A useful dynamic clamp tool to explore differences between *in vitro* and *in vivo* was contributed by Destexhe et al (2001), who demonstrated that the electrical portion of synaptic background activity might be approximated by Ornstein-Uhlenbeck processes (Chance and Abbot, 2009).

Modeling synaptic background activity in this way, which has been called the "point conductance" method, requires integrating stochastic (rather than deterministic) differential equations and generating Gaussian random numbers. In our example code, we demonstrate how to do these things. Two conductance trains, one representing excitatory inputs and the other representing inhibitory inputs, were generated independently as Ornstein–Uhlenbeck processes. Each was determined by an equation of the form:

$$\frac{dg(t)}{dt} = -\frac{1}{\tau}[g(t) - g_0] + \sqrt{D}\chi(t)$$

where g(t) is the value of the conductance, g_0 is its mean value, τ is a time constant, D is a "diffusion" constant, and $\chi(t)$ is a Gaussian white noise term of zero mean and unit standard deviation. As illustrated in Figure 8A (left), such an equation produces a random walk in time around the mean value, with a variance given by $\sigma^2 = D\tau/2$.

Introduction of this synaptic background activity had three distinct effects on the model cell (Fig. 8B): a depolarization of 5-10 mV, membrane potential fluctuations of ~10 mV, and a decrease in input

eNeuro Accepted Manuscript

resistance of more than a factor of 5. Varying the mean and standard deviation of the excitatory and/or inhibitory conductances produced changes in total conductance and membrane potential that closely matched what would be predicted given the model cell parameters (Fig. 8C).

Pyramidal neurons

We further tested the system using whole cell patch recordings from layer 2/3 and 5 pyramidal neurons in acute mouse prefrontal slices.

Layer 2/3 pyramidal neurons have relatively little HCN current, at least when compared with pyramidal neurons in deeper layers (Biel et al., 2009). As a result, they respond to temporally-fluctuating input as lowpass filters and they exhibit no or very small sag potentials. To test the first property, we injected a chirp stimulus (sinusoidal current with a frequency that increases in time, also known as a ZAP stimulus) into a layer 2/3 pyramidal neuron. As expected, the voltage deflection dropped as the frequency increased (Fig. 9A, left). We quantified this effect by calculating the impedance, which can be thought of as a frequency-dependent resistance, by dividing the Fourier transforms of the voltage and the current (Fig. 9A, upper right). The impedance decreased monotonically between 0 and 15 Hz. Into this neuron, we then introduced an HCN conductance of 6 nS using the dynamic clamp system. With this addition, the voltage deflection in response to the chirp stimulus showed a peak (a resonance) when the stimulus frequency was near 5 Hz (Fig. 9A, left and upper right, traces in red). In the absence of the simulated HCN conductance, this neuron showed no sag potential, but addition of the HCN conductance both reduced the steady-state resistance (smaller voltage deflection in response to a fixed current) and added a sag potential (Fig. 9A, lower right).

To first order, the intrinsic excitability of neurons turns on the balance between hyperpolarizing currents (especially leak) and depolarizing currents (especially transient sodium). (To second and higher order,

eNeuro Accepted Manuscript

many other types of currents enter in.) We increased the intrinsic excitability of a layer 2/3 pyramidal neuron by injecting 100 or 200 nS of simulated sodium conductance (Fig. 9B). A current step that was subthreshold in the basal state (left, trace in blue) produced one or six action potentials (left, traces in green and red) when sodium conductance amplitude was increased. Likewise, a current step that was just suprathreshold in the basal state (right) produced more and more spikes as sodium conductance amplitude was increased. Moreover, the latency to first spike and the threshold of the first spike dropped as sodium conductance was added.

In an acute slice, neurons exist in a quiescent state with spontaneous firing rates and V_m fluctuations near zero. This is very different than the active state that exists *in vivo* (Destexhe et al., 2003). We simulated an *in vivo*-like active state in a layer 5 pyramidal neuron in a brain slice using the point conductance method (Fig. 9C). The neuron's activity reproduced the expected features of high conductance state background activity: a firing rate of 2 Hz, a mean depolarization of 10 mV, and V_m fluctuations with a standard deviation of 5 mV.

Alternatives to Teensy

We built the dynamic clamp system around the Teensy 3.6 microcontroller because of its speed and memory, but the approach is more general. It is not limited to this particular device. In fact, many other microcontrollers could be used with only slight modifications to the code. To underline this point, in the online material (folder *Alternatives to Teensy*) we include software and instructions for using an Arduino Due or a chipKit uC32 in place of the Teensy 3.6. The first is a member of the Arduino line of microcontrollers (www.arduino.cc); the second is based on a separate family (called PIC) of microcontrollers (chipkit.net).

eNeuro Accepted Manuscript

DISCUSSION

We have here introduced a dynamic clamp system built around a microcontroller and suitable for addition to any intracellular electrophysiology rig. In designing the system, we were guided by three requirements: (1) low cost (<USD$100), (2) compatibility with the wide range of hardware and software found on existing rigs, and (3) accessibility to researchers with little prior experience with electronics or programming. The system not only meets these three requirements, but its performance is comparable in accuracy and speed to those posted by the leading alternatives (Destexhe and Bal, 2009; Prinz and Cudmore, 2011). It was able to simulate with an average error of only a few percent the same variety of conductances other systems have been used to simulate, and its single-conductance speed (90 kHZ) was exceeded by only 3 of 24 published systems (pre-2012 systems reviewed by Lin, 2012; Clausen et al., 2013; Yang et al., 2015).

The principal limitation on the accuracy of our system is that the ADC inputs and DAC outputs of the Teensy 3.6 microcontroller have 12 bit (4096 levels) precision, rather than the 16 bit (65536 levels) precision available in recent DAQ systems. While this is indeed a limitation, it is not (we would argue) an important one. Consider the ADC input: 12 bit precision means that the input's 3.3 V total range is sampled in increments of 0.8 mV. Given the empirical relationship between ADC input and membrane potential V_m (Fig. 3A), we were therefore able to measure V_m with a precision of 0.06 mV. For physiologically-realistic experiments, this is almost certainly good enough. And it is a lower limit: as we note in the online material (*Assembling the system*), one can adjust the resistor values to take better advantage of the ADC input's full dynamic range; our choices were conservative. An argument similar to the ADC one pertains to the DAC output.

A different potential limitation on accuracy – one that our system shares with most existing dynamic clamp systems (Destexhe and Bal, 2009) – arises from our use of forward Euler numerical integration for

eNeuro Accepted Manuscript

601 the Hodgkin-Huxley and Ornstein-Uhlenbeck equations (Bettencourt et al., 2008). However, our
602 simulation of the transient sodium conductance (Fig. 6) suggests that this is not a determinative
603 limitation. The reason that it is not is that the microcontroller can do the integration with a very fast
604 time step (<12 µs), which is fast enough to obviate most problems. It is possible to implement a more
605 precise numerical method on a Teensy-class microcontroller (see, e.g., http://bit.ly/2t6Jtyk), but this
606 would come at the cost of simulation speed. For example, employing the fourth-order Runge-Kutta
607 method would drop the speed by a factor of two. There is a tradeoff between accuracy and speed. Our
608 data indicate that, even for transient sodium, forward Euler is satisfactory given how fast the Teensy
609 microcontroller is.

610 The dynamic clamp system as a whole is fast because the microcontroller is doing nothing but
611 implementing dynamic clamp routines. It is not maintaining an operating system, interacting with a user,
612 updating a graphical interface, or implementing other unrelated routines. It is devoted exclusively to
613 dynamic clamp. In this, it is similar to earlier hardware implementations, such as those based on digital
614 signal processing boards (Desai et al., 2006; Olypher et al., 2006), but with much reduced cost and
615 complexity. Somewhat faster dynamic clamp systems have been introduced recently, including one
616 based on MATLAB's xPC Target software (Clausen et al., 2013; >125 kHz) and another that utilizes Igor
617 Pro software and National Instruments hardware (Yang et al., 2015; >100 kHz), but, for many potential
618 users, these would require substantial modification of existing electrophysiology systems, as well as the
619 purchase of new hardware and/or software.

620 In principle, the dynamic clamp system we describe could be made faster. On every cycle, the system
621 spends the bulk of its time doing two things: reading from the ADC input and writing to the DAC output.
622 One of our major goals was to keep the system as simple as possible, and so we used the built-in analog
623 read and write functions of the Teensyduino version of the Arduino language. However, a defining
624 feature of maker movement devices like the Teensy microcontroller – one that distinguishes them from

eNeuro Accepted Manuscript

many commercial devices – is that users have direct access to their inner workings; those innermost parts are not protected. One could reduce the time spent reading and writing the analog ports by addressing the registers directly and, for example, reducing how many samples the ADC input takes before reporting a result (see, e.g., https://github.com/pedvide/ADC). The cost of such a manipulation is in accuracy: it might increase noise. As always, there is tradeoff between accuracy and speed. A smaller improvement might be obtained by using higher quality electronic components. We chose the LM358 chip as an op-amp because of its ubiquity; it is available at nearly every hobbyist site. However, it has some limitations: it is not a "rail-to-rail" op-amp, which means that its behavior becomes erratic if the input voltages get close to the ±9 V rails of the power supply; it has a bandwidth and slew rate (how fast the voltage output can change in time) inferior to some other comparable op-amps (e.g., the OP484). Using these other op-amps would increase the cost of the system marginally (~USD$20), but might be worthwhile depending on the user's needs and would not degrade performance in any case.

Other microcontrollers (such as the Arduino Due, the top-of-the-line Arduino model) could be used in place of the Teensy 3.6 with only small modifications, but we chose the Teensy for three reasons. It has a clock speed equal to or faster than its competitors (180 MHz vs 84 MHz for the Due). It has more memory (256 kB RAM vs 92 kB for the Due). And it has a floating point unit (which all of the Arduino models lack). The last point is the most important. Microcontrollers of the Arduino class tend to omit a floating point unit, a piece of hardware dedicated to and optimized for arithmetic on numbers where the number of digits after the decimal point might vary. (The opposite of a floating point number is called a fixed point number, which has a fixed number of digits after the decimal point. An integer is the simplest example.) Variables naturally represented by float point numbers are ubiquitous in neurophysiology and particularly in Hodgkin-Huxley calculations. One might attempt to transform floating point arithmetic to fixed point arithmetic for the sake of speed (instead of asking what 2.0 x 2.00

eNeuro Accepted Manuscript

is, one might instead ask what 200 x 200 is and then divide the result by 10000), but the Teensy's architecture obviates the need for such machinations. Again, it keeps things simple.

eNeuro Accepted Manuscript

EXTENDED DATA

1. Parts list.

2. Assembling the system on a solderless breadboard.

3. Where to obtain and how to install Arduino and Processing.

4. Using and modifying Arduino software (including our Arduino code).

5. Using and modifying Processing software (including our Processing code).

6. Adding a potassium M conductance.

7. Matlab alternative to Processing.

8. Calibration procedure.

9. Alternatives to Teensy.

eNeuro Accepted Manuscript

660 **REFERENCES**

661

662 Anderson C. Makers: the new industrial revolution. New York: Crown, 2014.

663

664 Baden T, Chagas AM, Gage GJ, Marzullo TC, Prieto-Godino LL, Euler T. Open Labware: 3-D printing your
665 own lab equipment. PLoS Biology 13: e1002086, 2015.

666

667 Bettencourt JC, Lillis KP, White JA. Effects of imperfect dynamic clamp: computational and experimental
668 results. J Neurosci Methods 169:282-289 (2008).

669

670 Biel M, Wahl-Schott C, Michalakis S, Zong X. Hyperpolarization-activated cation channels: from genes to
671 function. Physiol Rev 89:847-885, 2009.

672

673 Biró I, Giugliano M. A reconfigurable visual-programming library for real-time closed-loop cellular
674 electrophysiology. Front Neuroinform 9:17, 2015.

675

676 Carnevale, T, Hines M. The NEURON book. New York: Cambridge University Press, 2009.

677

678 Chance FS, Abbott LF. Simulating in vivo background activity in a slice with the dynamic clamp. In:
679 Dynamic-clamp: from principles to applications. New York: Springer, 2009.

680

681 Clausen C, Valiunas V, Brink PR, and Cohen IS. MATLAB implementation of a dynamic clamp with
682 bandwidth >125 KHz capable of generating INa at 37°C. Pflugers Arch 465: 497–507, 2013.

683

eNeuro Accepted Manuscript

684 Compte A, Compte A, Brunel N, Goldman-Rakic PS, Wang XJ. Synaptic mechanisms and network
685 dynamics underlying spatial working memory in a cortical network model. Cereb Cortex 10:910-923,
686 2000.
687
688 Desai NS, Walcott EC. Synaptic bombardment modulates muscarinic effects in forelimb motor cortex. J
689 Neurosci 26: 2215-2226, 2006.
690
691 Desai NS, Siegel JJ, Taylor W, Chitwood RA, Johnston D. Matlab-based automated patch clamp system
692 for awake behaving mice. J Neurophysiol 114:1331-1345, 2015.
693
694 Destexhe A, Bal T (eds). Dynamic clamp: From principles to applications. New York: Springer, 2009.
695
696 Destexhe A, Mainen ZF, Sejnowski TJ. Synthesis of models for excitable membranes, synaptic
697 transmission and neuromodulation using a common kinetic framework. J Comput Neurosci 1:195–230,
698 1994.
699
700 Destexhe A, Rudolph M, Fellous JM, Sejnowski TJ. Fluctuating synaptic conductances recreate in vivo-like
701 activity in neocortical neurons. Neuroscience 107:13-24, 2001.
702
703 Destexhe A, Rudolph M, Paré D. The high conductance state of neocortical neurons in vivo. Nat. Rev.
704 Neurosci. 4:739-751, 2003.
705
706 Dorval AD, Christini DJ, White JA. Real-Time Linux Dynamic Clamp: A fast and flexible way to construct
707 virtual ion channels in living cells. Ann Biomed Eng 29:897-907, 2001.

eNeuro Accepted Manuscript

708

709 Finley K. Out in the open: the men supercharging neuroscience with open source hardware. Wired:
710 March 10, 2014.

711

712 Fransen E, Alonso AA, Hasselmo ME. Simulations of the role of the muscarinic-activated calcium-
713 sensitive nonspecific cation current INCM in entorhinal neuronal activity during delayed matching tasks.
714 J Neurosci 22:1081–1097, 2002.

715

716 Gasparini S, Migliore M, Magee JC. On the initiation and propagation of dendritic spikes in CA1
717 pyramidal neurons. J Neurosci 24:11046–11056, 2004.

718

719 Johnston D, Wu S. Foundation of cellular neurophysiology. Cambridge, MA: The MIT Press, 1994.

720

721 Kemenes I, Marra V, Crossley M, Samu D, Staras K, Kemenes G and Nowotny T. Dynamic clamp with
722 StdpC software. Nature Prot 6:405-417, 2011.

723

724 Kullmann PHM, Wheeler DW, Beacom J, Horn JP. Implementation of a fast 16-bit dynamic clamp using
725 LabVIEW-RT. J Neurophysiol 91:542-554, 2004.

726

727 Lin, RJ. Real-time methods in neural electrophysiology to improve efficacy of dynamic clamp. Ph.D.
728 dissertation, Georgia Institute of Technology, 2012.

729

730 Marsaglia G, Bray TA. A convenient method for generating normal variables. SIAM Review 6:260-264,
731 1964.

eNeuro Accepted Manuscript

732

733 Milescu LS, Yamanishi T, Ptak K, Mogri MZ, Smith JC. Real-time kinetic modeling of voltage-gated ion
734 channels using dynamic clamp. Biophys J 95:66-87, 2008.

735

736 Morozov E. Making it. The New Yorker: January 13, 2014.

737

738 Narayanan R, Johnston D. The h channel mediates location-dependence and plasticity of intrinsic phase
739 response in rat hippocampal neurons. J Neurosci 28:5846-5860.

740

741 Nowotny T, Szucs A, Pinto RD, Selverston AI. StdpC: a modern dynamic clamp. J Neurosci Methods
742 158:287-299, 2006.

743

744 Olypher A, Cymbalyuk G, Calabrese RL. Hybrid systems analysis of the control of burst duration by low-
745 voltage-activated calcium current in leech heart interneurons. J Neurophysiol 96:2857-2867, 2006.

746

747 Ortega FA, Butera RJ, Christini DJ, White JA, Dorval AD. Dynamic clamp in cardiac and neuronal systems
748 using RTXI. Methods Mol Biol 1183:327-354, 2014.

749

750 Pinto RD, Elson RC, Szucs A, Rabinovich MI, Selverston AI, Abarbanel HDI. Extended dynamic clamp:
751 controlling up to four neurons using a single desktop computer and interface. J Neurosci Meth 108:39-
752 48, 2001.

753

754 Potter SM, El Hady A, Fetz EE. Closed-loop neuroscience and neuroengineering. Front Neural Circuits
755 8:115, 2014.

eNeuro Accepted Manuscript

Prinz AA, Abbott LF, Marder E. The dynamic clamp comes of age. Trends Neurosci 27:218-224, 2004.

Prinz AA, Cudmore RH. Dynamic clamp. Scholarpedia: doi:10.4249/scholarpedia.1470, 2011.

Raikov I, Preyer AJ, Butera RJ . MRCI: A flexible real-time dynamic clamp system for electrophysiology experiments. J Neurosci Meth 132:109-123, 2004.

Robinson HPC, Kawai N. Injection of digitally synthesized synaptic conductance transients to measure the integrative properties of neurons. J Neurosci Meth 49:157-165, 1993.

Senturia SD, Wedlock BD. Electronic circuits and applications. New York: John Wiley & Sons, 1975.

Sharp AA, Abbott LF, Marder E. Artificial electrical synapses in oscillatory networks. J Neurophysiol 67:1691-1694, 1992.

Sharp AA, O'Neil MB, Abbott LF, Marder E. The dynamic clamp: artificial conductances in biological neurons. Trends Neurosci 16:389-394, 1993.

Siegle JH, Cuevas López A, Patel Y, Abramov K, Ohayon S, Voigts J. Open Ephys: an open-source, plugin-based platform for multichannel electrophysiology. J Neural Eng, 2017.

Steriade, M. The intact and sliced brain. Cambridge, MA: MIT Press, 2001.

eNeuro Accepted Manuscript

780 Teikari P, Najjar RP, Malkki H, Knoblauch K, Dumortier D, Gronfier C, Cooper HM. An inexpensive
781 Arduino-based LED stimulator system for vision research. J Neurosci Meth 211: 227-236, 2012.
782
783 Walcott EC, Higgins EA, Desai NS. Synaptic and intrinsic balancing during postnatal development in rat
784 pups exposed to valproic acid in utero. J Neurosci 31: 13097-13109, 2011.
785
786 Yang Y, Adowski T, Ramamurthy B, Neef A, Xu-Friedman MA. High-speed dynamic-clamp interface. J
787 Neurophysiol 113:2713-2720, 2015.
788
789
790

eNeuro Accepted Manuscript

FIGURE CAPTIONS

Figure 1. Schematic representations of the system. (A) The Teensy 3.6 microcontroller and its associated electronics (RED) are added to an existing system (BLACK) consisting of an intracellular amplifier and a data acquisition (DAQ) system. The amplifier sends the membrane potential V_m to both the DAQ system and the Teensy system. The DAQ system, which could (for example) be comprised of a Digidata 1500 and pClamp 10 software, records V_m to disk as usual and specifies whatever current (I_{CC}) it would inject in a standard current-clamp configuration. The microcontroller uses V_m to calculate what current (I_{DC}) the dynamic clamp conductances would have passed had they been physically present. The sum of these two currents, $I_{AMP} = I_{CC} + I_{DC}$, is sent to the command input of the amplifier to be injected into the neuron. (B) The Teensy system consists of five parts: (1) a power supply 18 V, which is broken up into a positive voltage (+9 V) and a negative voltage (-9 V) to power the other circuits and to provide both positive and negative rails; (2) a differential amplifier circuit that maps the output of the intracellular amplifier, which will be in the range ±9 V, onto the range 0-3.3 V that the Teensy can read; (3) the Teensy controller itself; (4) a second differential amplifier circuit that maps the output of the Teensy, which will be in the range 0-3.3 V, onto the range ±9 V the intracellular amplifier expects at its command input; and (5) a summing circuit that adds the voltage commands representing I_{CC} and I_{DC}. A voltage representing the sum I_{AMP} is sent to the intracellular amplifier and thereafter injected into the neuron. (C) The entire system can be built on a standard solderless breadboard. The five parts of the system are indicated by the arrows. All of the components (resistors, capacitors, ICs, wires, and microcontroller) can be secured simply by pushing their wires into the breadboard holes; no soldering is required. A detailed, step-by-step description of how to assemble the five parts of the system on a breadboard is available in the Extended Data (document titled *Assembling the system on a solderless breadboard*).

eNeuro Accepted Manuscript

Figure 2. Breadboard electronics. The five parts of the system illustrated in Fig. 1B are shown schematically. (A) Rail splitter power supply. An 18 V power supply (wall adaptor) is split by a TLE 2426 rail splitter IC into +9 V, -9 V, and ground. The capacitors are C_1=200 µF and C_2=1 µF. The dark numbers refer to the pins of the TLE 2426 IC. (B) Follower, voltage divider, and differential amplifier circuits to transform ±9 V to approximately 0-3.3 V. The resistor values are R_1=2200 Ω, R_2=470 Ω, R_3=4700 Ω, R_4=22000 Ω, R_5=10000 Ω, and R_6=100 Ω. (C) Connections to the Teensy 3.6 microcontroller. The output of the previous circuit is fed to pin A0, the output of pin DAC0 is fed to the next circuit. (D) Differential amplifier circuit to transform the output of the microcontroller (0-3.3 V, representing the dynamic clamp current) into a range (±9 V) expected by the intracellular amplifier. The resistor values are R_7=4700 Ω, R_8=22000 Ω, R_9=10000 Ω, and R_{10}=10000 Ω. (E) Summing amplifier. The voltage command from the DAQ board (representing the current clamp's specified current) is added to the voltage command from the Teensy microcontroller. The sum is sent to the command input of the intracellular amplifier. Resistors R_{11}, R_{12}, R_{13}, R_{15}, and R_{16} are 10000 Ω; resistor R_{14} is 3300 Ω; and R_{17} is 4700 Ω.

Figure 3. Calibrating and testing the system. (A) Even though the electronic components were not ideal, the input-output characteristics of the system were highly linear. Left: the voltages measured by the microcontroller's analog input in response to a range of membrane potentials. Right: the currents injected into a model cell in response to a range of voltages sent out by the microcontroller's analog output. (B) To test the system, a model cell was attached to the intracellular amplifier's headstage. Shown is the model's equivalent circuit. (C) The system's speed approaches 100 kHz and depends only weakly on the number of conductances being simulated. We recorded the durations of 51200 time steps (at microsecond resolution) for each of three dynamic clamp configurations: shunt conductance only; shunt, HCN, and sodium conductances together; and shunt, HCN, sodium, Ornstein-Uhlenbeck, and EPSC conductances all together. Shown in the three figures at left are the resulting histograms; the number

eNeuro Accepted Manuscript

at the top of each is mean ± SD. The temporal jitter in all cases was 1-2 µs. To check the temporal latency, sinusoidal voltages (5 kHz) were fed to the system's input (replacing V_{IN} of Fig. 2B) and the resulting outgoing current commands (V_{AMP} of Fig. 2E) were measured for a shunt conductance (2 nS). Both the input signal and the output signal were sampled at 100 kHz. The latency between input and output was roughly 10 µs.

Figure 4. Shunt conductance. Adding 5 nS of shunt conductance to the model cell reduced and quickened the voltage deflections to a family of current steps (upper left). The shunt currents added by the dynamic clamp system (measured directly by the DAQ board) closely matched what they should have been given the recorded membrane potentials (numerical) (upper right). The inset shows a probability histogram of the difference (error) between the measured and numerical currents. Varying the amplitude of the shunt conductance affected the input resistance and time constant (measured) as expected given the numerical values of the model cell resistance and the shunt conductance amplitudes (numerical) (lower panels).

Figure 5. HCN conductance. (A) The conductance was modeled by a single activation gate that had a steady-state value $s_{inf}(V)$ and a time constant $\tau_s(V)$. (B) Currents steps (-100 to +40 pA) were injected into a model cell without (CTL) and with (+ HCN) the addition of +2 nS HCN conductance. Note that adding the simulated conductance resulted in the appearance of a "sag" potential (left). At right, the currents injected by the dynamic clamp system (measured, directly by the DAQ board) for the eight steps are plotted together with the result of numerically integrating the Hodgkin-Huxley equation using the 4th order Runge-Kutta method (numerical). The top histogram ("steps error") of panel *D* shows how good the agreement between the measured and predicted (numerical) currents was. (C) The model cell (Fig. 3B) is essentially an "RC circuit." In response to a time-varying input, it acts like a lowpass filter. This

eNeuro Accepted Manuscript

can be seen (left) by its response to a chirp stimulus (black); the voltage deflection steadily decreases as the frequency increases. Addition of +4 nS HCN conductance transforms the system into a bandpass filter, with a resonant frequency. Again, the agreement between the current injected by the dynamic clamp system (measured) and the expected current given by numerical integration of the Hodgkin-Huxley equations (numerical) was excellent. (D) Histograms of the error between the measured and expected currents for step currents (top) and the chirp current (bottom).

Figure 6. Sodium conductance. (A) The conductance was modeled using both an activation gate $m(V_m,t)$ and an inactivation gate $h(V_m,t)$. The steady-state and kinetic values of the two gates are plotted. The total sodium current was given by $g_{Na}m^3h(V_m-E_{Na})$, where g_{Na} is the maximal sodium conductance and E_{Na} is the sodium reversal potential (+50 mV). (B) A comparison of different numerical integration methods. In a simulation, the voltage was stepped instantaneously from -70 mV to 0 mV at a time t = 20 ms. The resulting (inward) sodium current was calculated using the forward Euler method (timestep 200, 100, or 12 µs), the 4th order Runge-Kutta method (timestep 10 µs), or by an exact analytical calculation (exact). For the Euler simulation of 12 µs, the timestep was also jittered by 2 µs (standard deviation). (C) At left, the response of the model cell to slow current ramps (5, 10, and 20 pA/s) is plotted in the absence (CTL) and the presence (+ Na) of an added sodium conductance (g_{Na}=20 nS). In the middle, the close agreement between the sodium currents produced by the dynamic clamp system (measured) and those expected from precise numerical integration of the Hodgkin-Huxley equations (numerical) is demonstrated. At right is a histogram of the error (difference) between the measured and expected currents. (C) The model cell was subjected to brief current steps. Without a sodium conductance, the responses showed pure exponential growth, as expected of an RC circuit. With a sodium conductance (g_{Na}=80 nS), the responses showed non-linear behavior above a threshold (>25 pA). The sodium currents (measured directly and expected from numerical integration) are plotted in the middle. Not only do the

eNeuro Accepted Manuscript

887 currents agree with each other, but they show a striking threshold behavior. At right (top), the error
888 (difference) between the measured current and the expected current is plotted for the largest current
889 step (100 pA). The shape of the error is consistent with what would be expected from a small offset in
890 the baseline membrane potential. At right (bottom) is the difference between the 4^{th} order Runge-Kutta
891 (timestep 10 μs) estimate of the current for a baseline of -70 mV and the estimate for a baseline of -69.5
892 mV.
893
894 **Figure 7.** Excitatory postsynaptic currents (EPSCs). (A) EPSCs were triggered at fixed times with
895 stimulation frequencies of 10, 20, and 50 Hz. Note how the potentials summate for the higher
896 frequencies. (B) The agreement between the currents injected by the dynamic clamp system (measured)
897 and the expected currents given by precise Runge-Kutta numerical integration of the two-stage kinetic
898 scheme we employed for EPSCs (Compte et al., 2000) was excellent at all frequencies. (C) A histogram of
899 the difference (error) between the measured and expected currents. Data from all three frequencies
900 were combined in this histogram.
901
902 **Figure 8.** Synaptic background activity. (A) In the "point conductance" model of Destexhe et al. (2001),
903 synaptic background activity is modeled by two noisy conductance trains. One represents excitatory
904 input, the other represents inhibitory input; both are generated by Ornstein-Uhlenbeck processes. Each
905 train is normally distributed (middle) and is correlated at short times (right; the power spectrum goes
906 like $1/f^2$ for higher frequencies). (B) Without background activity, the model cell has a flat membrane
907 potential (left) that is almost constant (middle); its input resistance is large (right). Adding "in-vivo-like"
908 background activity depolarizes the membrane, introduces membrane potential fluctuations, and
909 reduces the input resistance. The vertical scale of the middle histogram is truncated so that the
910 membrane potential distribution in the active state is easier to see. (C) Varying the mean (g, in nS) and

eNeuro Accepted Manuscript

standard deviation (s, in nS) of the excitatory and inhibitory conductances produced the predicted changes in total conductance (top) and membrane potential fluctuations (bottom). The added conductance is expected to equal the sum of gE and gI. The numerical estimates of V_m standard deviation were calculated by simulating the model cell. When sE and sI were varied, gE and gI were held fixed at 4 nS.

Figure 9. Dynamic clamp recordings from pyramidal neurons in slices of mouse prefrontal cortex. (A) HCN conductance. Left: a layer 2/3 pyramidal neuron shows a lowpass filtering response (blue) when subjected to a chirp current (black). This is transformed into a bandpass response (red) when 6 nS HCN conductance is added by the dynamic clamp. Upper right: the impedance profiles show this effect quantitatively. Lower right: the neuron also developed a sag potential in response to hyperpolarizing current injections. (B) Sodium conductance. Addition of 100 or 200 nS of sodium conductance makes this layer 2/3 pyramidal neuron more excitable in a graded fashion. Shown are the responses to current steps of 50 and 100 pA. (C) Synaptic background activity in a layer 5 pyramidal neuron. The point conductance method was used to simulate an "*in vivo*-like" state (excitatory mean 3 nS, excitatory standard deviation 1.5 nS, inhibitory mean 6 nS, inhibitory standard deviation 3 nS). At left is a 5 sec recording of membrane potential V_m. At right is a histogram of subthreshold membrane potential; the spikes of the 5 sec recording were clipped out, and the remainder were used to construct the histogram.

eNeuro Accepted Manuscript

A

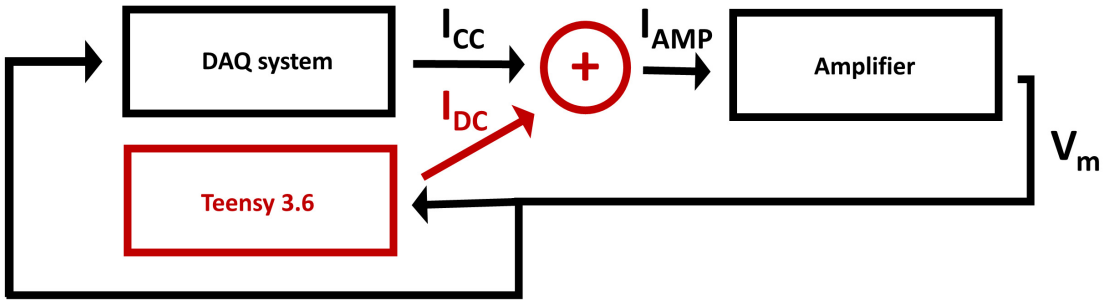

B

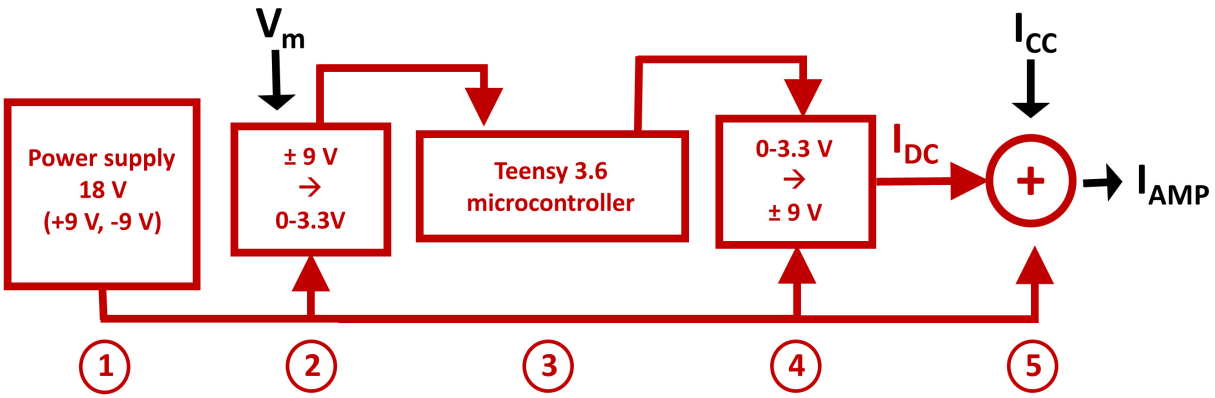

C

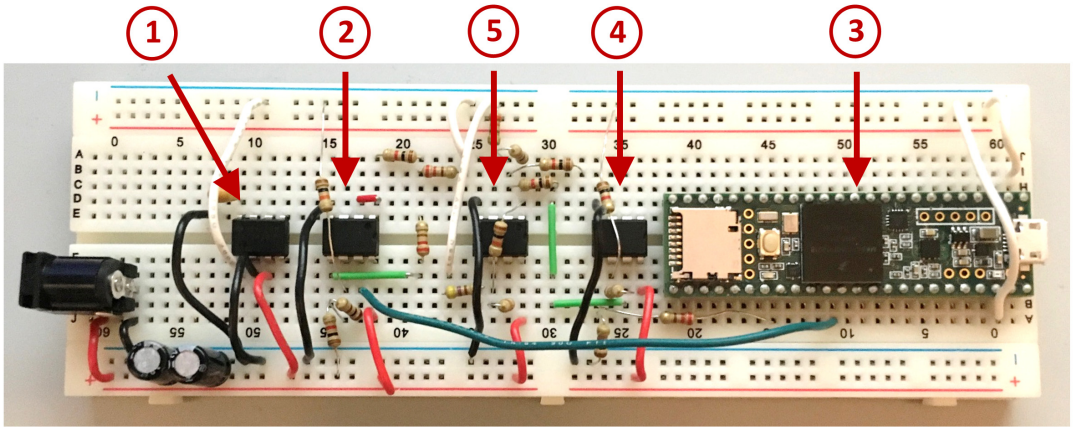

eNeuro Accepted Manuscript

A

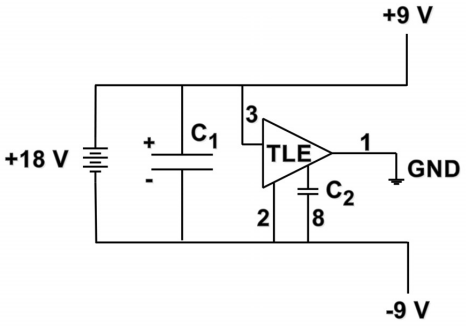

B

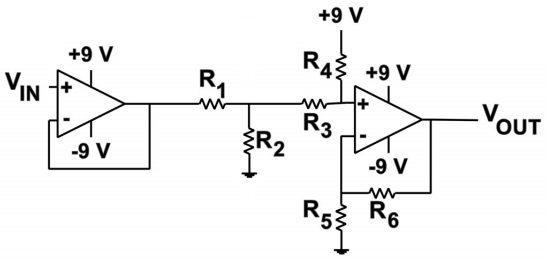

C

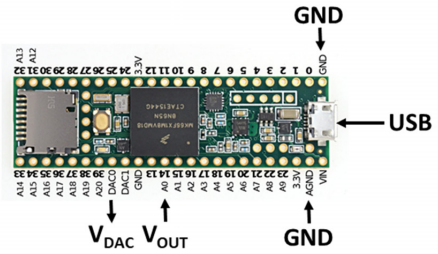

D

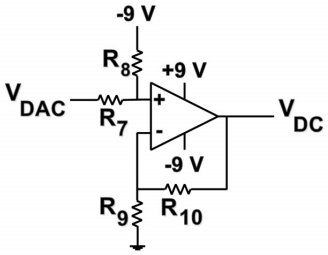

E

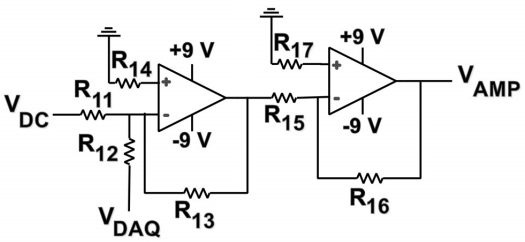

eNeuro Accepted Manuscript

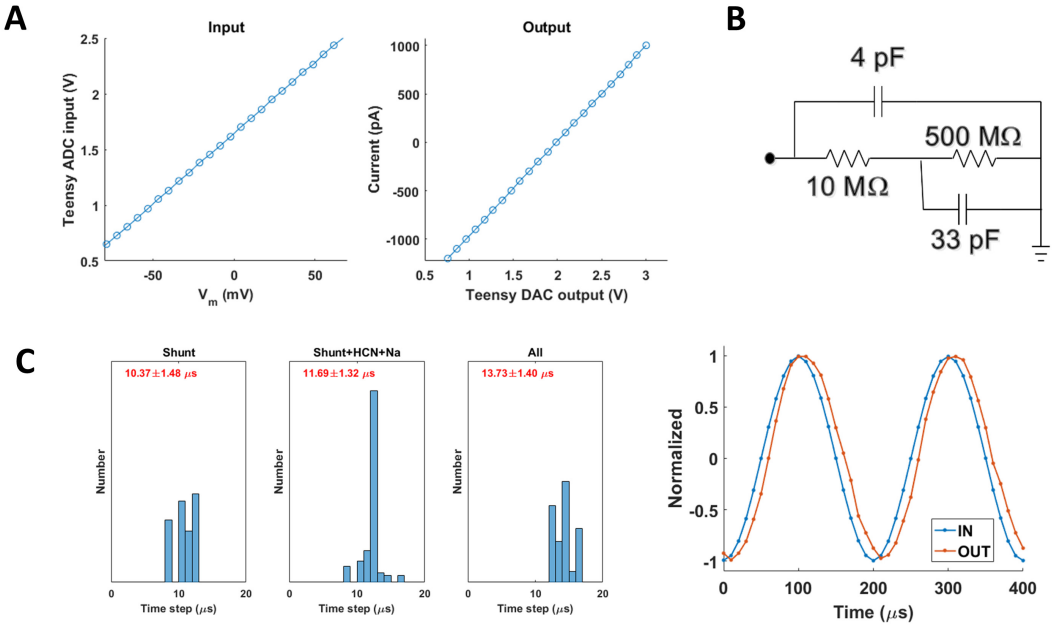

eNeuro Accepted Manuscript

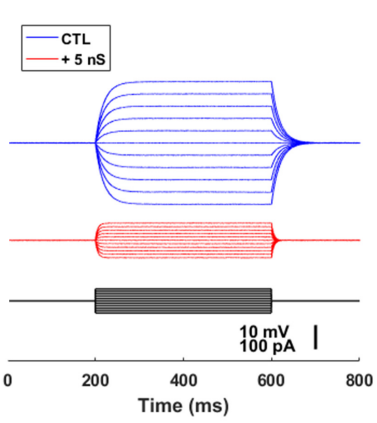

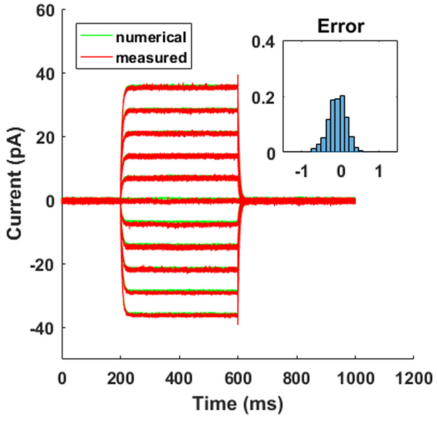

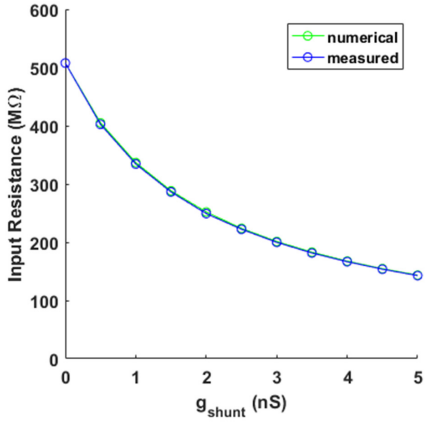

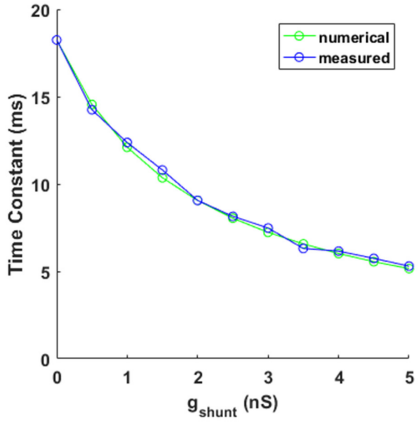

eNeuro Accepted Manuscript

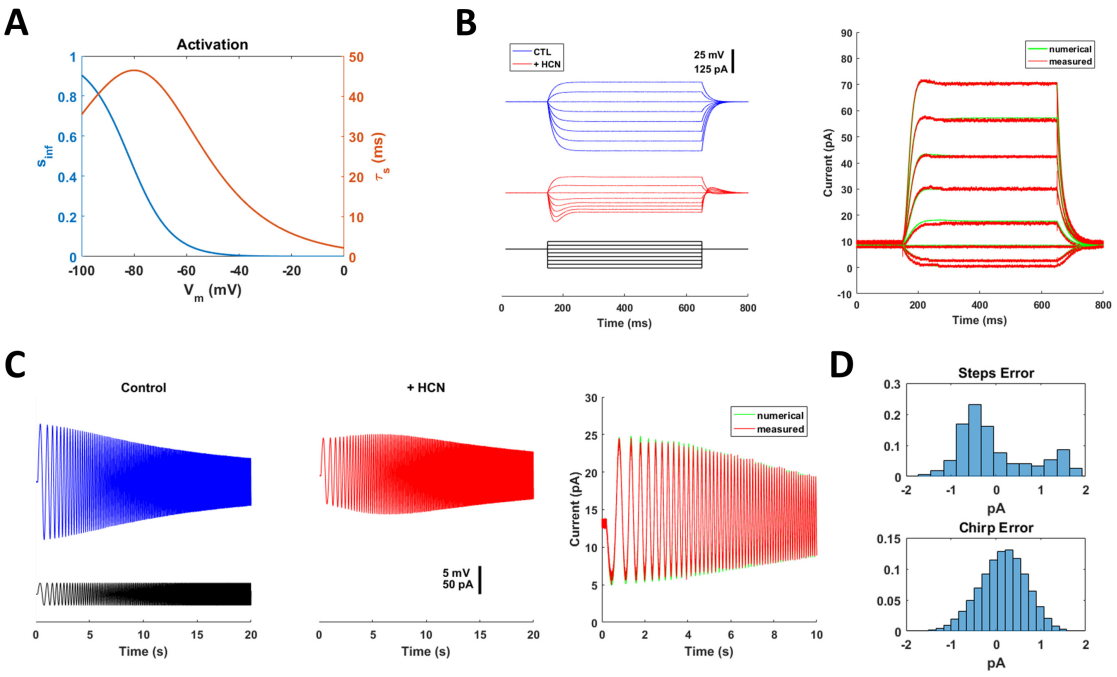

eNeuro Accepted Manuscript

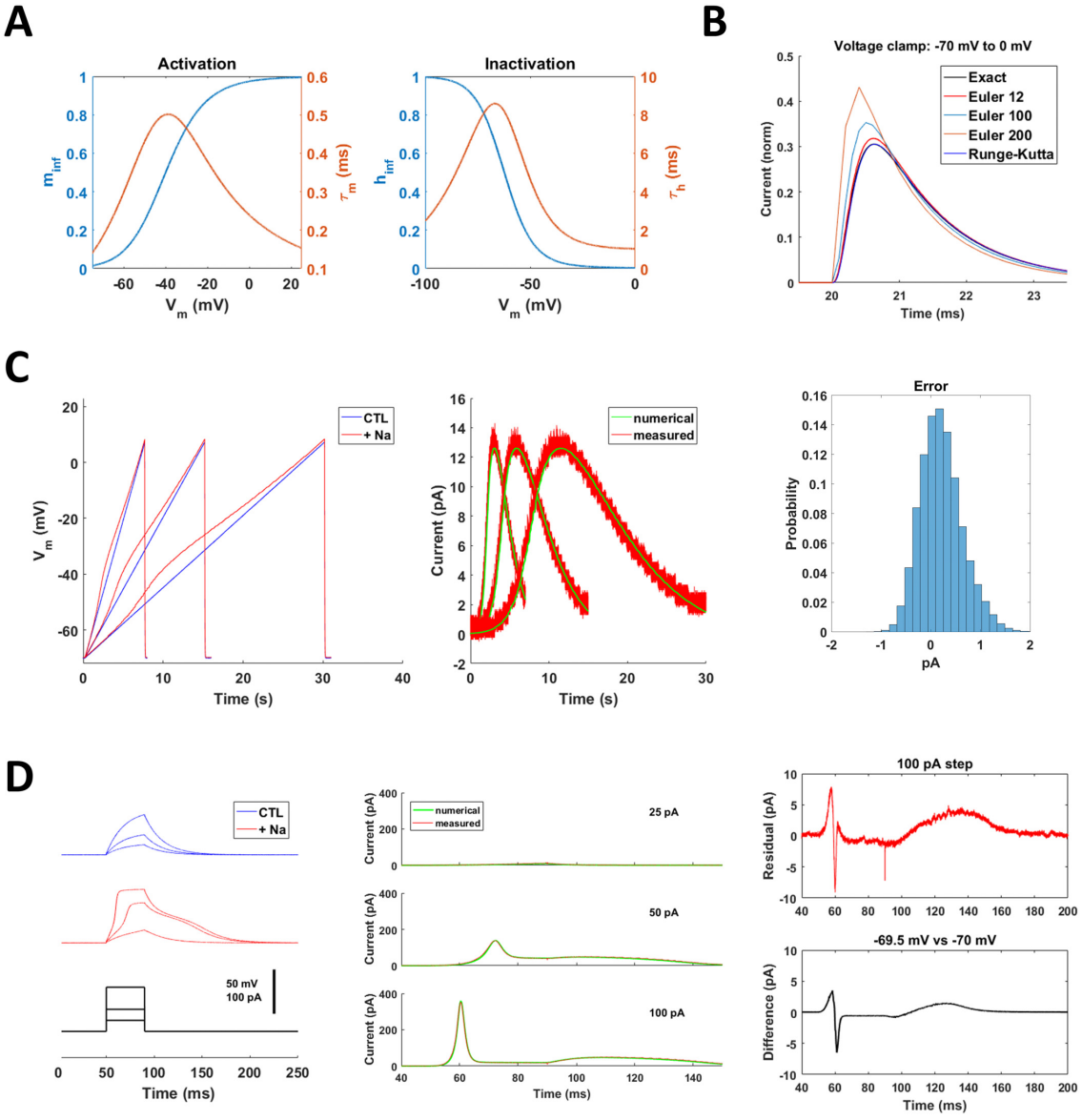

eNeuro Accepted Manuscript

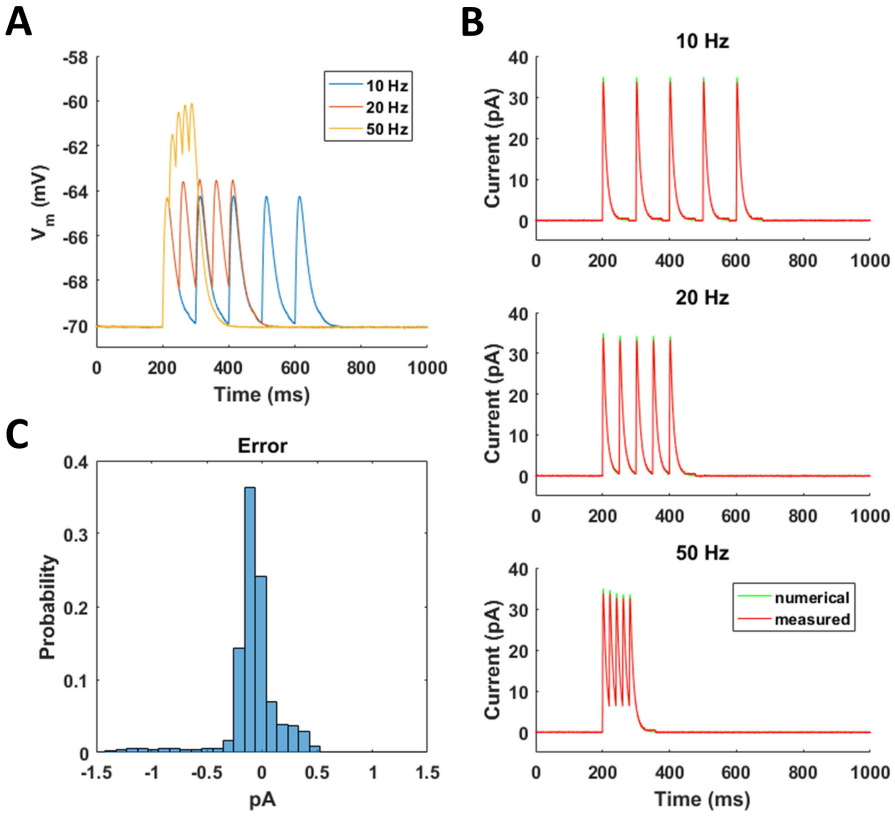

eNeuro Accepted Manuscript

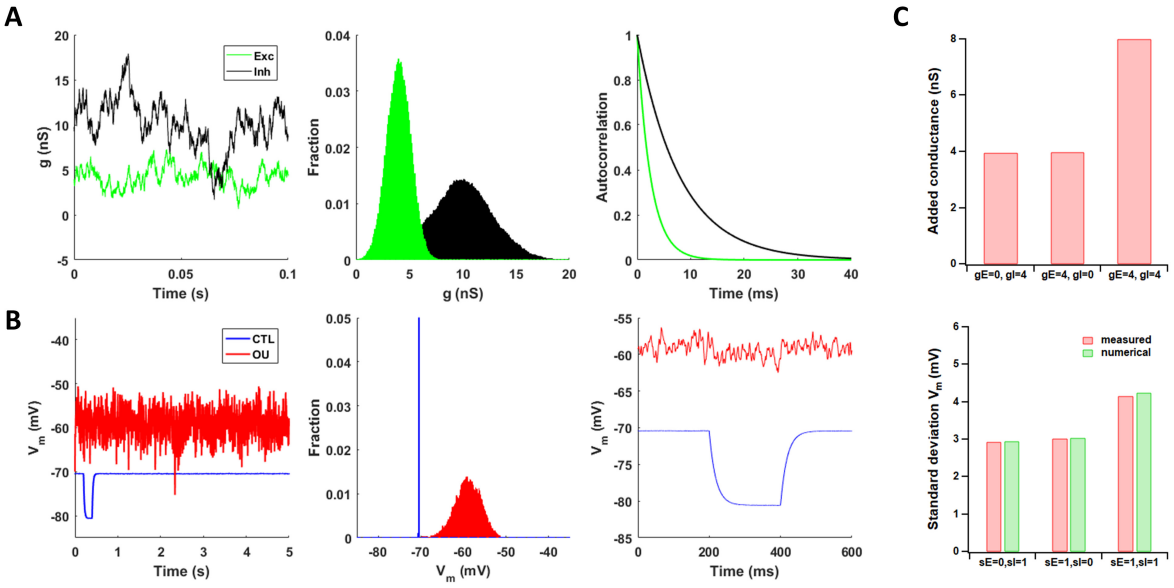

eNeuro Accepted Manuscript